mathematics

MDPI

Article

Torricelli's Law in Fractal Space–Time Continuum

Didier Samayoa [1], Liliana Alvarez-Romero [1], José Alfredo Jiménez-Bernal [1], Lucero Damián Adame [2], Andriy Kryvko [1] and Claudia del C. Gutiérrez-Torres [1,*]

[1] Instituto Politécnico Nacional, SEPI-ESIME Zacatenco, Unidad Profesional Adolfo López Mateos, Mexico City 07738, Mexico; dsamayoa@ipn.mx (D.S.); lalvarezr1501@alumno.ipn.mx (L.A.-R.); jjimenezb@ipn.mx (J.A.J.-B.); akryvko@ipn.mx (A.K.)

[2] Computational Robotics Department, Universidad Politécnica de Yucatán, Carretera Mérida-Tetiz, Km. 4.5, Ucú 97357, Mexico; lucero.damian@upy.edu.mx

* Correspondence: cgutierrezt@ipn.mx

Abstract: A new formulation of Torricelli's law in a fractal space–time continuum is developed to compute the water discharge in fractal reservoirs. Fractal Torricelli's law is obtained by applying fractal continuum calculus concepts using local fractional differential operators. The model obtained can be used to describe the behavior of real flows, considering the losses in non-conventional reservoirs, taking into account two additional fractal parameters α and β in the spatial and temporal fractal continuum derivatives, respectively. This model is applied to the flows in reservoirs with structures of three-dimensional deterministic fractals, such as inverse Menger sponge, Sierpinski cube, and Cantor dust. The results of the level water discharge $H(t)$ are presented as a curve series, showing the impact and influence of fluid flow in naturally fractured reservoirs that posses self-similar properties.

Keywords: Torricelli's law; fractal continuum; Menger sponge; Sierpinski cube; discharge velocity

MSC: 26A33

check for updates

Citation: Samayoa, D.; Alvarez-Romero, L.; Jiménez-Bernal, J.A.; Damián Adame, L.; Kryvko, A.; Gutiérrez-Torres, C.d.C. Torricelli's Law in Fractal Space–Time Continuum. *Mathematics* **2024**, *12*, 2044. https://doi.org/10.3390/math12132044

Academic Editor: Jonathan Blackledge

Received: 22 May 2024
Revised: 21 June 2024
Accepted: 29 June 2024
Published: 30 June 2024

Copyright: © 2024 by the authors. Licensee MDPI, Basel, Switzerland. This article is an open access article distributed under the terms and conditions of the Creative Commons Attribution (CC BY) license (https://creativecommons.org/licenses/by/4.0/).

1. Introduction

Fractional operators have become a powerful alternative framework to describe physical phenomena employing non-integer dimensions and sometimes non-standard measures in complex domains where ordinary calculus is no longer valid [1]. Many advances in fractional calculus have been developed to solve real-world problems, such as transport in porous media [2–5], viscoelasticity [6–8], elastodynamics [9,10], diffusion [11–13], biomechanics [14], image encryption [15], vehicular traffic flow [16], sociophysics [17,18], and quantum theory [19–21], to mention a few.

Recent reports claim that this approach is suitable for establishing the constitutive relationship of time-dependent viscoelastic material behavior, which leads to fractional derivative models as a generalized form of classical derivatives that take into account self-similarity and fractional dimension properties [22].

In this regard, several methodologies have been developed to describe the behavior of fractal materials more efficiently, such as fractal geometry [23–25], local fractal calculus [26,27], and fractal continuum [28–30].

Therefore, the gravity-driven discharge from natural reservoirs and aquifers that possess self-similarity properties can be modeled with these techniques. Particularly, a generalization of the law proposed by the Italian Evangelista Torricelli [31] from Euclidean to fractal space continuum is introduced in this work.

The fractal continuum approach is employed to deduce the influence of fractality in non-conventional reservoirs, particularly on the velocity of the outgoing water flow, through a hole at the bottom of the container. Specifically, the fractal continuum calculus

F^{α}-*CC*, suggested in [32,33] is considered, as it includes both geometry and fractal topology through Hausdorff (d_H) and chemical (d_{ch}) dimensions, respectively [34]. Moreover, F^{α}-*CC* incorporates other fractal dimensions [35] such as spectral dimension d_s, which is defined by the relationship $\Omega(\omega) \sim \omega^{d_s - 1}$, being $\Omega(\omega)$ the density of fractal vibration modes with frequency ω in the fractal domain, and the fractal dimension of the shortest pass $d_{min} = d_H / d_{ch}$ linked to its fractal topology [36].

It is well known that in the integer space–time, Torricelli's law for water discharge velocity U is given by [31,37]:

$$U = \sqrt{2gH}, \tag{1}$$

where H is the water level in the reservoir and g is the gravitational acceleration.

Equation (1) applies to Euclidean reservoirs and aquifers whose shapes are ideally smooth and regular. However, the domains of many natural reservoirs have a complicated architecture, usually very irregular, complex, and scale-invariant [38,39]. This implies that the above equation is insufficient to describe the hydrological processes in these domains in detail.

A fractal modification of Torricelli's law was suggested in Ref. [40], in which the coefficient $1/(1 + V_0^{d_H - 3})$ is introduced to take into account the mechanical energy loss, where V_0 is the initial volume of water in the reservoir and d_H is the fractal dimension of the reservoir. Thus, the modified fractal of Torricelli's equation is:

$$U = \frac{1}{1 + V_0^{d_H - 3}} \sqrt{2gH}, \tag{2}$$

which leads to a better description of fluid behavior than the Euclidean equation.

Subsequently, it was experimentally established that the instantaneous water discharge rate Q obeys the kinematic wave flux law in complex domains such as balls folded from square aluminum foils of different thicknesses and edge sizes [41].

Recently, a comparative study of water discharge from Euclidean and fractal reservoirs was carried out [42], where it was found that the water discharge is governed by Bernoulli's principle instead of Darcy's law [5,43–45], where the Torricelli's discharge from the fractal reservoir is larger than that from the Euclidean ones.

The main objective of this work is to map Torricelli's law from ordinary to fractal space-time continuum to solve the problem of water discharge in non-conventional reservoirs with a fractal formulation capable of describing its behavior in detail. The fractal Torricelli's law is developed and numerically implemented in the fractal reservoir with a structure of inverse Sierpinski cube, Menger sponge, and Cantor dust types, which are presented in the next sections.

The fractal model proposed is of great interest due to its possible applications in real-world engineering, such as civil engineering, petroleum engineering, geomechanics, hydrogeology, transport in porous media, and watershed-aquifer modeling and monitoring, where the characterization of complex and amorphous reservoirs with irregular geometries is well described using the concepts of F^{α}-*CC*.

The rest of the paper is outlined as follows. Section 2 is devoted to developing the main subject of this work, i.e., the mapping of Toricelli's law in a fractal continuum. Section 3 presents the applications of the developed fractal formulation. In Section 4, a discussion of mechanical implications is carried out, and Section 5 finishes the paper with conclusions.

2. Generalization of Torricelli's Law from Conventional to Fractal Calculus

This section is devoted to deducing the generalized Torricelli's law in fractal space–time continuum using F^{α}-CC.

2.1. Definition of Fractal Continuum Derivatives

Fractal continuum calculus is a generalized version of classical calculus, which implies the mapping of physical problems in non-differentiable fractal media into the corresponding problems in the fractal continuum using local differential operators. Thus, the functions defined in the fractal continuum space–time become differentiable in the ordinary sense, allowing non-conventional local derivatives to be expressed in terms of ordinary derivatives (see Figure 1). To achieve this, the F^{α}-CC was developed with its own fractional norm, metrics, and measure. Moreover, it has rules for integrodifferential calculus and its own Laplacian, which are summarized as follows [46]:

i The fractional norm is defined as $\| N \| = \left[\sum_k^3 \xi_k^{2\gamma}\right]^{1/2\gamma}$, where $\gamma = d_{ch}/3 \leq 1$ and the mapping of the fractional coordinates in the fractal continuum $\xi_k \in \mathcal{F}^{\alpha}$ from the Cartesian coordinates in the embedding Euclidean space $x_k \in E^3$ is given by

$$\xi_k = \ell^{1-\alpha_k} x_k^{\alpha_k}, \tag{3}$$

where $\alpha_k = d_H - d_A$ is the fractal dimension in the fractional direction ξ_k (see Figure 1), d_A denotes the Hausdorff dimension of cross-section, and ℓ is the lower cutoff of the fractal domain.

ii The distance between two points $A, B \in \mathcal{F}^{\alpha}$ is defined by $\Delta(A, B) = \left[\sum_k^3 \Delta_k^{2\gamma}\right]^{1/2\gamma}$, with $\Delta_k = \| \xi_{ak} - \xi_{bk} \|$.

iii The gradient operator is expressed as $\nabla^{d_H} = \mathbf{e}_k \nabla_k^{d_H}$, where $\mathbf{e}_k$ are basis vectors, and

$$\nabla_k^{d_H} = \left(\frac{1}{\alpha_k \ell^{1-\alpha_k} x_k^{\alpha_k - 1}}\right) \nabla_k, \tag{4}$$

is the definition of the spatial fractal continuum derivative.

iv Meanwhile, the divergence operator is given by $\nabla^{d_H} \cdot \vec{F}$.

v So, the Laplacian is $\Delta^{\alpha} = \nabla^{\alpha} \left(\nabla^{\alpha} \cdot F\right) = \sum_k^3 \frac{2}{\alpha_k \ell^{1-\alpha_k} x_k^{\alpha_k - 1}} \left[\nabla_k^2 + \frac{\gamma - \alpha_k}{x_k} \nabla_k\right] F$.

vi The time fractal continuum derivative is defined by

$$\nabla_t^H = \left(\frac{t}{\tau} + 1\right)^{1-\beta} \nabla_t, \tag{5}$$

where $\beta = d_s / d_H$ is the fractal dimension of time and τ is an adjustment parameter called characteristic time.

These local operators define the density, displacement, temperature, etc., as analytic envelopes of non-analytic functions in order to describe the properties of the fractal under study, for example, by applying the scaling transformation from Cartesian coordinates into fractal continuum coordinates; the fractal continuum displacement δ_k is given by:

$$\delta_k = \alpha_k \ell^{1-\alpha_k} x_k^{\alpha_k - 1} u_k, \tag{6}$$

where u_k is the integer space–time displacement. In Figure 1, a geometrical illustration of this mapping is shown.

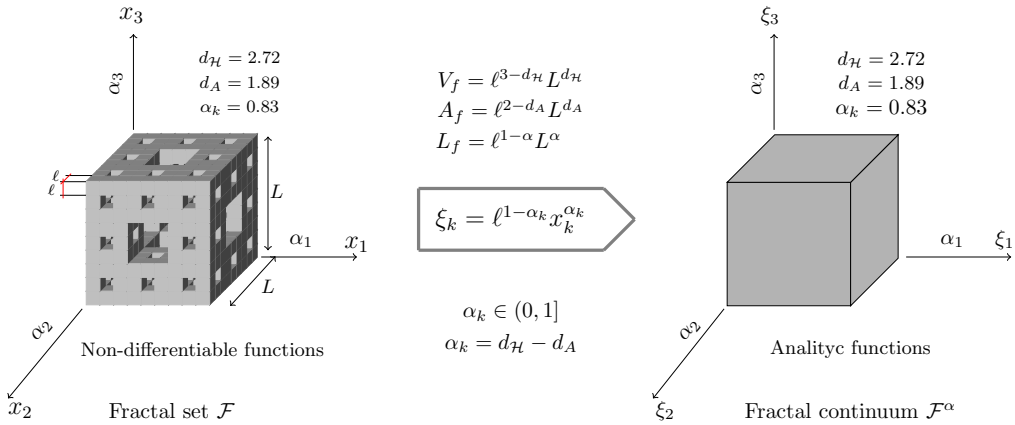

Figure 1. Geometrical interpretation of fractal continuum calculus using classical Menger sponge.

2.2. Fractal Continuum Torricelli's Law

Conventional Torricelli's law can be mapped from integer to fractal space–time continuum using Equation (5), as follows:

$$\mathbb{U} = \sqrt{2g\ell^{1-\alpha}H^{\alpha}}, \tag{7}$$

where $\mathbb{U}$ represents the fractal water velocity at the hole and H is the fractal water level in the reservoir, so Equation (7) is a generalized (fractal) Torricelli's law. Note that Equation (7) reduces to the conventional Torricelli's law (1), when the Hausdorff dimension α in the direction of H is equal to one. A mechanical representation of fractal Torricelli's law is depicted in Figure 2, derived from Equation (7) for four different alpha values and $0 \leq H \leq 0.27$, as shown in Figure 3.

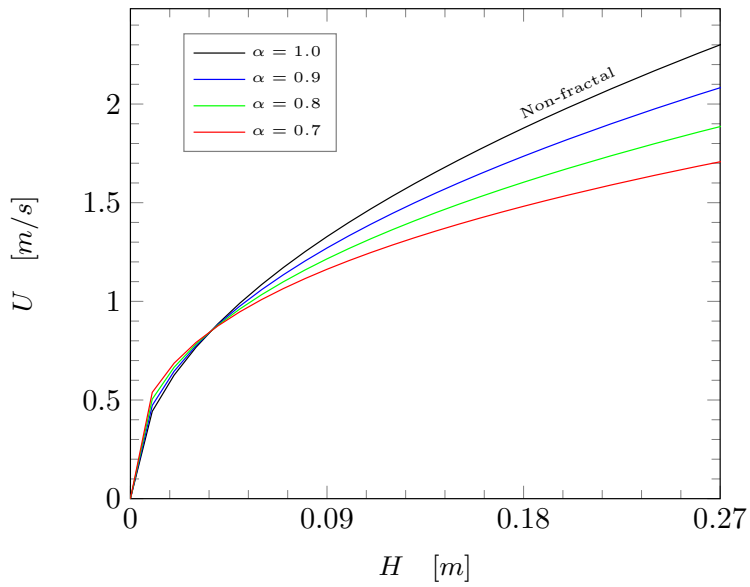

Figure 2. The effect of fractional orders α on the discharge velocity from the generalized Toricelli's Equation (7).

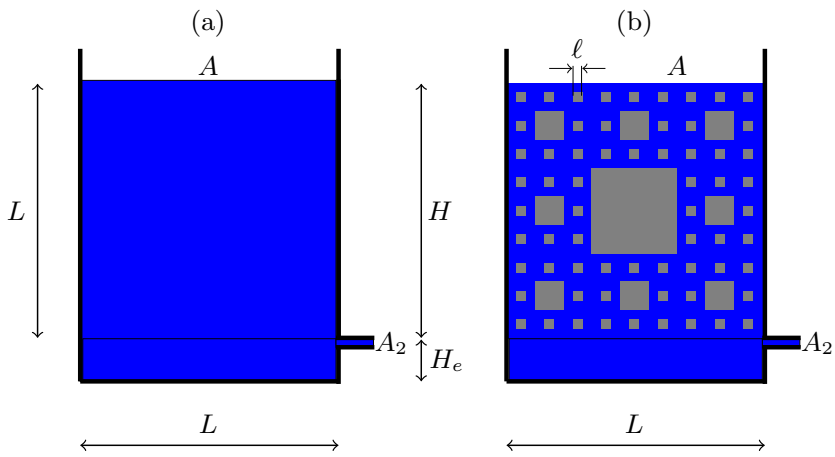

Figure 3. Configurations of reservoirs: (**a**) Euclidean and (**b**) fractal.

On the other hand, from the mass conservation equation (see the geometrical illustration of Figure 3), the following can be calculated:

$$A\frac{dH}{dt} + A_2\sqrt{2gH} = 0, \tag{8}$$

where A is the cross-section area of the reservoir and A_2 is the water exit area, so its fractal generalization can be obtained by substituting Equations (3) and (5) into Equation (8), thus obtaining:

$$\left(\frac{t}{\tau}+1\right)^{1-\beta}\frac{dH}{dt} = \frac{-A_2}{A}\sqrt{2g\ell^{1-\alpha}H^{\alpha}}. \tag{9}$$

Equation (9) can be rewritten as:

$$H^{-\frac{\alpha}{2}}dH = -\frac{A_2}{A}\sqrt{2g\ell^{1-\alpha}}\left(\frac{t}{\tau}+1\right)^{1-\beta}dt, \tag{10}$$

By integrating Equation (10), we have:

$$\left(\frac{1}{1-\frac{\alpha}{2}}\right)H^{1-\frac{\alpha}{2}}\,|_0^t = -\frac{A_2}{A}\sqrt{2g\ell^{1-\alpha}}\left[\left(\frac{t}{\tau}+1\right)^{\beta}-1\right], \tag{11}$$

For $H(0) = H_e$, we obtain:

$$H(t) = \left[H_e^{1-\frac{\alpha}{2}} - \left(1-\frac{\alpha}{2}\right)\frac{A_2}{A}\sqrt{2g\ell^{1-\alpha}}\left[\left(\frac{t}{\tau}+1\right)^{\beta}-1\right]\right]^{\frac{2}{2-\alpha}}. \tag{12}$$

It is straightforward to see that if $\alpha = \beta = \tau = 1$, then Equation (12) converts to its conventional (Euclidean) form, i.e.,:

$$H(t) = \left(\sqrt{H_e} - \frac{A_2}{2A}\sqrt{2g}\,t\right)^2, \tag{13}$$

In Figure 4, the impact of fractional orders of α and β on water discharge described by Equation (12) is plotted. The Euclidean discharge is obtained when α and $\beta = 1$ are both equal to one.

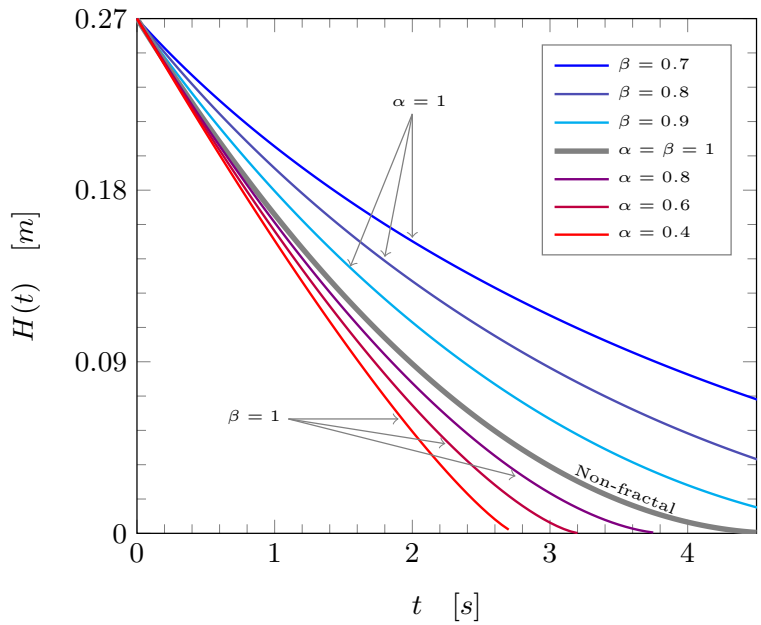

Figure 4. Water level curves from Equation (12) for different values of α and β: the curves above the gray curve are such that $\alpha = 1,\ \beta \in [0,1)$; at the gray curve, $\alpha = \beta = 1$; and the curves below the gray curve are such that $\alpha \in [0,1),\ \beta = 1$ (with $A/A_2 = 170$).

3. Theoretical Implementation of Fractal Formulation

The objective of this section is to validate the fractal continuum formulation developed by applying it to fractal reservoirs of known geometries, such as the inverse Sierpinski cube, Menger sponge, and Cantor dust types.

3.1. Fractal Reservoirs

Classical Menger sponge features are well known [47]. It is constructed from the unit cube $[0,1]^3 \subset \Re^3$, which is divided into $\epsilon \times \epsilon \times \epsilon$ sub-cubes of equal sizes. Then, the interiors of the sub-cubes are eliminated. In each one of the remaining sub-cubes, the same operation is repeated. This procedure is iterated ad infinitum [47]. The fractal parameters of the classical Menger sponge are shown in Table 1.

Table 1. Fractal parameters of considered reservoirs.

Reservoir	d_H	d_{ch}	d_s	d_A	α	β	L (m)	ℓ (m)
Sierpinski cube	$\frac{\log 540}{\log 9}$	d_H	2.76	$\frac{\log 72}{\log 9}$	0.91	0.97	0.27	0.03
Menger sponge	$\frac{\log 20}{\log 3}$	d_H	$\frac{3\log 20}{\log 34}$	$\frac{\log 8}{\log 3}$	0.83	0.93	0.27	0.03
Cantor dust 1	$\frac{\log 216}{\log 7}$	3	3	$\frac{\log 36}{\log 7}$	0.92	1.08	0.27	0.03
Cantor dust 2	$\frac{\log 8}{\log 3}$	3	3	$\frac{\log 4}{\log 3}$	0.63	1.58	0.27	0.03
Euclidean	3	3	3	2	1	1	0.27	0.27

The Sierpinski carpet and Sierpinski cube are one of various two- and three-dimensional versions of the Cantor set, respectively, whose Hausdorff dimension is defined as [48]:

$$d_H = \frac{d\, log[N(\epsilon) - B]}{log[N(\epsilon)]}, \tag{14}$$

where $N(\epsilon)$ denotes the number of boxes covering the fractal whose size is $\epsilon = L/\ell$, and B is the number of deleted boxes of the fractal mass; meanwhile, d represents the dimension

of Euclidean space, where the fractal is embedded. Note that for $d = 1$, the fractal is the Cantor set and the boxes are segments of length ϵ; for $d = 2$, the fractal is a Sierpinski carpet and the size of each box is a square $\epsilon \times \epsilon$, whereas if $d = 3$, it is the Sierpinski cube and the box is a cube $\epsilon \times \epsilon \times \epsilon$.

It has been demonstrated that when the geodesic and Euclidean metrics are equivalent, as, for example, the Sierpinski and Menger sponge fractals, their chemical dimensions are equal to their Hausdorff dimensions $d_{ch} = d_H$ [49]. Meanwhile, for any three-dimensional Cantor dust, which is a path-disconnected fractal, its chemical dimension is equal to three [50]. In this regard, the Cantor dust also has a spectral dimension equal to its chemical dimension $d_{ch} = d_s = 3$.

On the other hand, the spectral dimension of the Sierpinski cube and Menger sponge is computed by [51]

$$d_s = \frac{3\,log[N(\epsilon) - B]}{log[N(\epsilon) + B]}. \tag{15}$$

3.2. The Properties and Characteristics of the Studied Reservoirs

In Table 1, the values of different dimensional numbers and other parameters of three-dimensional fractals used in non-conventional reservoirs are presented.

3.3. Implementation

The model is used to analyze fractal media with the characteristics described in Table 1. Equation (12) is applied to two different types of fractal reservoirs: (a) path-connected fractals, specifically the inverse Sierpinski cube and Menger sponge, and (b) totally disconnected fractals, such as three-dimensional Cantor dust. Figure 5 displays the water discharge behavior, illustrating the impact fractality for each type of fractal reservoir considered.

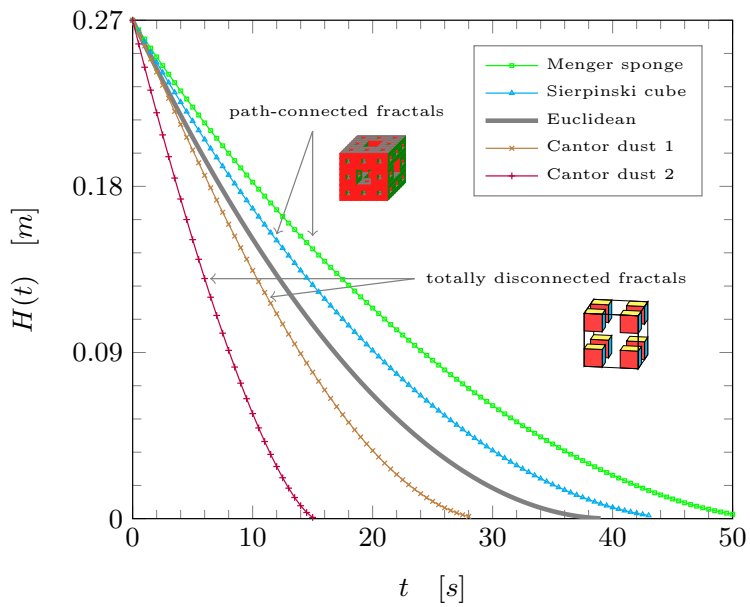

Figure 5. Water discharge for different fractal reservoirs with data shown in Table 1.

The unidimensional version of the Sierpinski cube studied in this work is a Cantor set with a middle interval of 3/9, and its Hausdorff dimension obtained from Equation (14) is $d_H = \log[9-3]/\log 9$.

Two cases of Cantor dust with different initiators are considered. The first one is the classical Cantor dust with a middle interval of length 1/3 with $d_H = \log 2/\log 3$, and the

second Cantor dust is constructed with a middle interval of length $1/7$, whose Hausdorff dimension in its unidimensional version is $d_H = \log 2/[\log 2 - \log(1 - 1/7)]$.

In Figure 6, the influence of fractal parameters of the classical Menger sponge in the reservoir using different iterations $k = 0, 1, 2, 3, 4$ is sketched using Equation (12) and the data from Table 1.

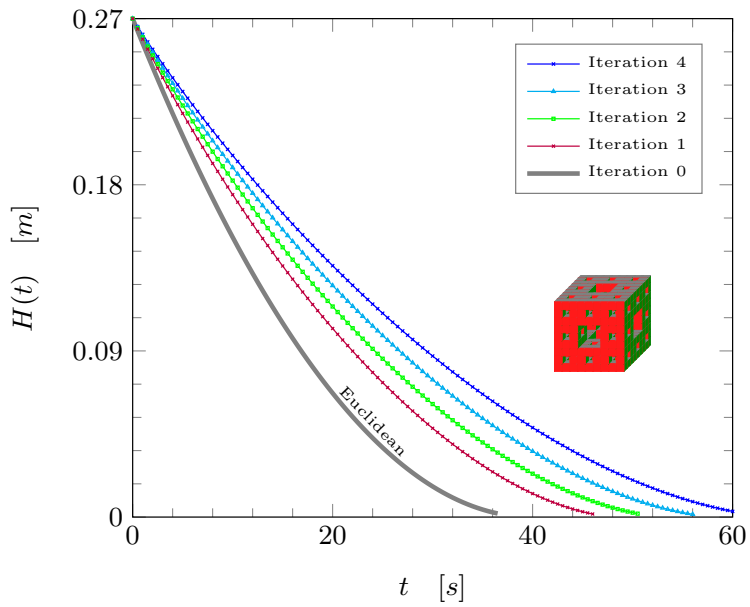

Figure 6. Water discharge in the reservoirs of classical inverse Menger sponge types with $\alpha = 0.83$ and $\beta = 0.93$ for iterations 0,1,2,3,4 (iteration zero represents an Euclidean reservoir, where $\alpha = \beta = 1$).

4. Analysis and Discussion of Results

4.1. Numerical Evaluation of Fractal Formulations

The water discharge from fractal reservoirs with path-connected fractal structures is larger than in the Euclidean reservoir, as shown in Figure 5 in green and cyan colors for the Menger sponge and Sierpinski cube, respectively. This behavior is in accordance with the experimental results published in [42] and validates our fractal formulation. In the real world, non-conventional reservoirs have channels and porous networks similar to path-connected fractals, so the water flow can be explained by the results obtained for the fractal reservoirs with Sierpinki cube and Menger sponge fractal structures.

Moreover, in Figure 5, there are curves that lie below the Euclidean water discharge, and such curves do not represent real-world water discharge behavior. That is why flows in reservoirs with path-disconnected fractal geometry are not physically reproducible in non-conventional reservoirs.

The curves in Figure 6 are more distant from the Euclidean discharge curve as the iteration of the Menger sponge increases; in each iteration, the fractal mass increases (as the fractional part of the reservoir is the inverse of the Menger sponge), which implies that the channel and porous volumes decrease as the iteration number increases.

On the other hand, the efflux time for fractal and Euclidean reservoirs can be obtained from Equation (11) as:

$$t_e = \tau \left[\left\{ \left(\frac{1}{1 - \frac{\alpha}{2}} \right) \frac{A}{A_2} \left[\frac{H^{1-\frac{\alpha}{2}}}{\sqrt{2g\ell_0^{1-\alpha}}} - \frac{H_e^{1-\frac{\alpha}{2}}}{\sqrt{2g\ell_0^{1-\alpha}}} + \left(1 - \frac{\alpha}{2}\right) \frac{A_2}{A} \right] \right\}^{\frac{1}{\beta}} - 1 \right]. \tag{16}$$

The conventional t_e is:

$$t_e = \frac{A}{A_2}\left[\sqrt{\frac{2H}{g}} - \sqrt{\frac{2H_e}{g}}\right], \tag{17}$$

which can be obtained from the extended-form Equation (16) for $\alpha = \beta = 1$. The behavior for the case of a reservoir of a classical inverse Menger sponge type is presented in Figure 7. It can be observed that the efflux time in the Euclidean reservoir is shorter than in the fractal reservoir of the inverse Menger sponge type, which matches the results found in Ref. [40].

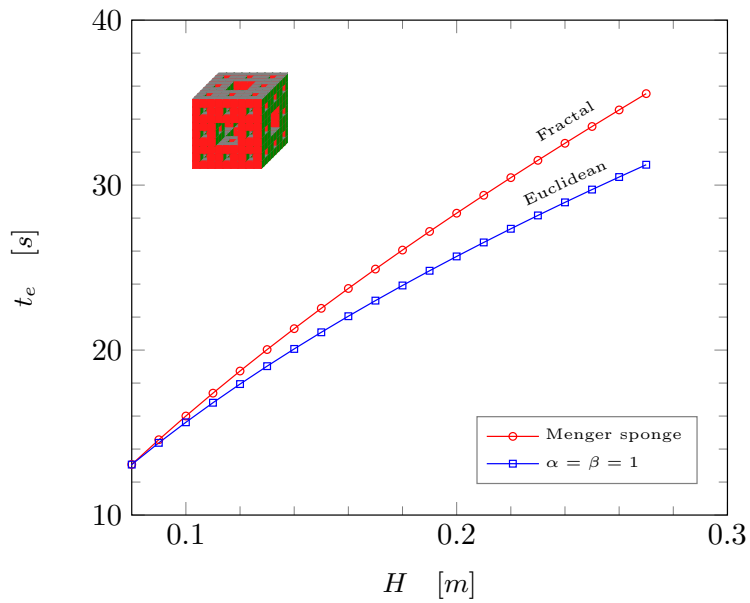

Figure 7. Efflux time for the fractal and the Euclidean reservoirs versus the initial water level ($A/A_2 = 170$).

Moreover, the fractal continuum model of Torricelli's law proposed in this work does not have physical inconsistency, as the fractal Torricelli's law deduced in [40] has the fractal coefficient $1/(1 + V_0^{d_H-3})$, which must be equal to one when the reservoir is Euclidean ($d_H = 3$). Equations (7), (12), and (16), suggested in this work, simplify to the standard forms when the Hausdorff and spectral dimensions are both equal to three and the Hausdorff dimension of cross-section area is equal to two. Consequently, we have $\alpha = d_H - d_A = 1$, and similarly, $\beta = d_s/d_H = 1$. This is feasible because the Euclidean formulation is actually a specific case of the fractal formulation.

4.2. The Physical Motivations of the Fractal Continuum Approach

The driving motivation for the study of variable-order fractional operators is that these operators have the capability to describe physical systems whose properties are time-dependent. Such operators provide detailed descriptions in many practical applications, such as the water discharge from Torricelli's point of view.

Torricelli's fractal law incorporates three advantages over the traditional methodologies. Firstly, it employs fractional dimensions in fractional calculus; secondly, it uses the Hausdorff measure instead of the distance, as in ordinary calculus; and finally, it takes into account, in addition to the fractal geometry, a set of fractional dimensions that describe the fractal topology of the object under study.

A fractal formulation that only includes the Hausdorff dimension is incomplete because it only measures the complexity or roughness of this type of shape (as the Hausdorff dimension can be treated as the degree to which a set "fills" the Euclidean space in which the fractal object is immersed). However, there are fractals that have the same Hausdorff

dimension and can have different ramifications, connectivities, and dynamical properties (see Figure 8). This implies that some alternative models lead to very different solutions to the same problems for physical fractal domains.

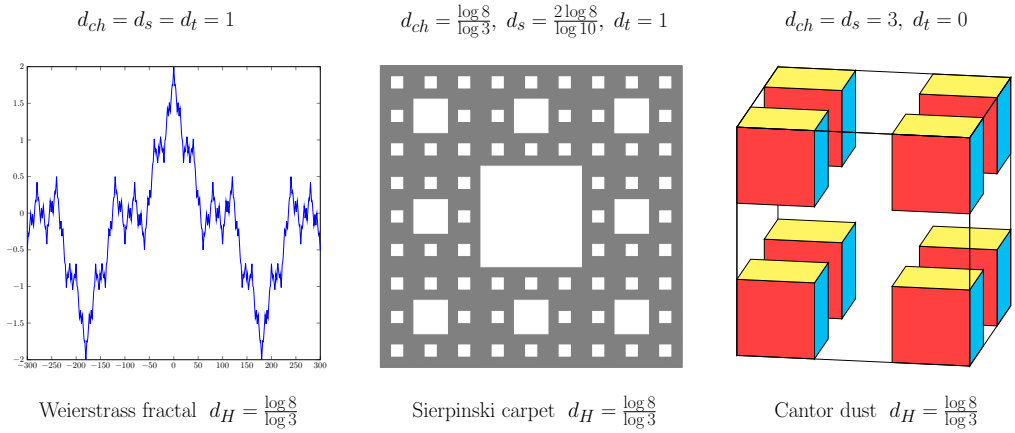

Figure 8. Fractal sets with the same Hausdorff dimension and different chemical, topological, and spectral dimensions (zero value of topological dimension in the Cantor dust describes a totally disconnected fractal.

Fractal features are characterized by the chemical dimension d_{ch}, spectral dimension d_s, topological dimension d_t, and topological Hausdorff dimension d_{tH}, among others. It has been argued that a complete description of the topological and geometrical features of a fractal set can be quantified by six independent dimension numbers [52].

The formulation suggested in this work includes the six dimensional numbers shown in Table 1, which allows us to describe, in more detail, the behavior of Torricelli's flow.

The proposed formulation can be utilized to fit field measurement data, which would otherwise require a laborious task to obtain the fractal parameters α and β. To do this, at first, the Hausdorff, topological, and cross-sectional area dimensions must be acquired through methods such as mercury intrusion [53,54], magnetic resonance [55], or statistical analysis [56,57]. Subsequently, the spectral and chemical dimensions should be determined by using numerical approximations [36] and/or theoretical relations [51].

On the other hand, Torricelli's equation relates the speed of a fluid flow through an orifice to the height of fluid above the opening. The law states that the speed of efflux of a fluid through a sharp-edged hole at the bottom of the tank filled to a certain level is the same as the speed that a body would acquire in free falling. Its validity can be extended to outflows from tanks filled with granular or fractured media. In some cases, the modified formula could be used as an alternative to Darcy's law, for example, in natural reservoirs and karst aquifers.

5. Conclusions

In this work, the impact of fractality in non-conventional reservoirs for the estimation of Torricelli's discharge is studied. A new fractal formulation of Torricelli's law is developed using fractional operators, specifically the fractal continuum approach, which takes into account the topological, morphological, and topographical properties of fractal domains through their Hausdorff, chemical, spectral, topological, and shortest path dimensions.

In the formulation proposed, two fractal parameters are introduced: the parameter $\alpha_k = d_H - d_A$, which is the Hausdorff dimension in the fractional direction of fractal space $\xi_k \in \mathbf{E}^3$, and the Hausdorff dimension of time scale $\beta = d_s/d_H$, which characterizes the fractal properties of fractal domains.

The behaviors of fractal discharge velocity and water level are plotted in Figures 2 and 4, respectively. The validation of the obtained behaviors was performed for fractal reservoirs with known dimensional numbers, such as inverse Sierpinski cube, Menger sponge, and

Cantor dust, and the obtained results match the experimental results previously reported in the literature.

It was found that the formulation proposed is physically consistent, and it is capable of efficiently predicting Torricelli's phenomena in reservoirs with fractal structures. Both Torricelli's discharge and efflux time in reservoirs are computed. Also, it was found that Torricelli's discharge is smaller in Euclidean reservoirs than in the fractal ones.

In an upcoming report, we will expand the mapping of Torricelli's law to a more generalized form known as the Bernoulli equation. An experimental analysis will also be performed on sample cores of rock, sandstone, and glass bead pack.

Author Contributions: Writing—original draft preparation, D.S.; writing—review and editing, J.A.J.-B., C.d.C.G.-T. and L.D.A.; conceptualization, A.K. and L.A.-R.; methodology, A.K. and C.d.C.G.-T.; software, J.A.J.-B. and L.A.-R.; formal analysis, D.S. and A.K.; visualization, L.A.-R. and L.D.A.; supervision, C.d.C.G.-T. and L.D.A. All authors have read and agreed to the published version of the manuscript.

Funding: This work was supported by the Instituto Politécnico Nacional under SIP-IPN research grant Nos. 20240111, 202040485, 20241305, and 20241354.

Institutional Review Board Statement: Not applicable.

Informed Consent Statement: Not applicable.

Data Availability Statement: All data are contained within the paper, and a report of any other data is not included.

Acknowledgments: The second author would like to express gratitude to the SENER-Conacyt scholarship for doctoral studies.

Conflicts of Interest: The authors declare no conflicts of interest.

References

1. Golmankhaneh, A. *Fractal Calculus and Its Applications*; World Scientific: Singapore, 2022.
2. Singh, J.; Kumar, D.; Kumar, S. An efficient computational method for local fractional transport equation occurring in fractal porous media. *Comp. Appl. Math.* **2020**, *39*, 137. [CrossRef]
3. Fuentes, C.; Alcántara-López, F.; Quevedo, A.; Chávez, C. Fractional Vertical Infiltration. *Mathematics* **2021**, *9*, 383. [CrossRef]
4. Su, N. *Fractional Calculus for Hydrology, Soil Science and Geomechanics: An Introduction to Applications*; Taylor and Francis Group, LLC: Boca Raton, FL, USA; London, UK; New York, NY, USA, 2022.
5. Damian-Adame, L.; Gutiérrez-Torres, C.; Figueroa-Espinoza, B.; Barbosa-Saldaña, J.; Jiménez-Bernal, J. A Mechanical Picture of Fractal Darcy's Law. *Fractal Fract.* **2023**, *7*, 639. [CrossRef]
6. Di-Paola, M.; Heuer, R.; Pirrota, A. Fractional visco-elastic Euler–Bernoulli beam. *Int. J. Solids Struct.* **2013**, *50*, 3505–3510. [CrossRef]
7. Cai, W.; Chen, W.; Xu, W. Characterizing the creep of viscoelastic materials by fractal derivative models. *Int. J. Non-Linear Mech.* **2016**, *87*, 58–63. [CrossRef]
8. Samayoa, D.; Damián, L.; Kryvko, A. Map of bending problem for self-similar beams into fractal continuum using Euler-Bernoulli principle. *Fractal Fract.* **2022**, *6*, 230. [CrossRef]
9. Kumar, S.; Chauhan, R.; Momani, S.; Hadid, S. A study of a modified nonlinear dynamical system with fractal-fractional derivative. *Int. J. Numer. Methods Heat Fluid Flow* **2022**, *32*, 2620–2639. [CrossRef]
10. El-Nabulsi, R.; Anukool, W. Fractal dimension modeling of seismology and earthquakes dynamics. *Acta Mech.* **2022**, *233*, 2107–2122. [CrossRef]
11. Balankin, A.S.; Baltasar, M.; Martínez-González, C.L.; Morales, D. Random walk in chemical space of Cantor dust as a paradigm of superdiffusion. *Phys. Rev. E* **2012**, *86*, 052101. [CrossRef]
12. Golmankhaneh, A.K.; Ochoa-Ontiveros, L. Fractal calculus approach to diffusion on fractal combs. *Chaos Solitons Fractals* **2023**, *175*, 114021. [CrossRef]
13. Zhukov, D.; Otradnov, K.; Kalinin, V. Fractional-Differential Models of the Time Series Evolution of Socio-Dynamic Processes with Possible Self-Organization and Memory. *Mathematics* **2024**, *12*, 484. [CrossRef]
14. Golmankhaneh-Amirreza, K.; Tunc, S.; Schlichtinger, A.M.; Asanza, D.M.; Golmankhaneh, A.K. Modeling tumor growth using fractal calculus: Insights into tumor dynamics. *Biosystems* **2024**, *235*, 105071. [CrossRef]
15. Wang, S.; Hong, L.; Jiang, J.; Li, X. Synchronization precision analysis of a fractional-order hyperchaos with application to image encryption. *AIP Adv.* **2020**, *10*, 105316. [CrossRef]

16. Dubey, V.; Kumar, D.; Alshehri, A.; Dubey, S.; Singh, J. Computational Analysis of Local Fractional LWR Model Occurring in a Fractal Vehicular Traffic Flow. *Fractal Fract.* **2022**, *6*, 426. [CrossRef]
17. Yu, X.; Zhang, Y.; Sun, H. Modeling COVID-19 spreading dynamics and unemployment rate evolution in rural and urban counties of Alabama and New York using fractional derivative models. *Results Phys.* **2021**, *26*, 104360. [CrossRef]
18. Shikongo, A. 11 A COVID-19-related Atangana-Baleanu Fractional Model for Unemployed Youths. In *Mathematical and Computational Modelling of COVID-19 Transmission*; River Publishers: New York, NY, USA, 2023; pp. 215–240.
19. Dubey, V.; Kumar, D.; Singh, J.; Alshehri, A.; Dubey, S. Analysis of local fractional Klein-Gordon equations arising in relativistic fractal quantum mechanics. *Waves Random Complex Media* **2022**, 1–21. [CrossRef]
20. Dubey, S.; Chakraverty, S. Hybrid techniques for approximate analytical solution of space- and time-fractional telegraph equations. *Pramana J. Phys.* **2023**, *97*, 11. [CrossRef]
21. Al-Raeei, M. Applying fractional quantum mechanics to systems with electrical screening effects. *Chaos Solitons Fractals* **2021**, *150*, 111209. [CrossRef]
22. Dubey, V.; Singh, J.; Alshehri, A.; Dubey, S.; Kumar, D. Analysis and Fractal Dynamics of Local Fractional Partial Differential Equations Occurring in Physical Science. *J. Comput. Nonlienar Dyn.* **2023**, *18*, 031001. [CrossRef]
23. Falconer, K. *Fractal Geometry: Mathematical Foundations and Applications*; John Wiley and Sons, Ltd.: Chichester, UK, 2014.
24. Carpinteri, A.; Chiai, B.; Cornetti, P. A fractal theory for the mechanics of elastic materials. *Chaos Soliton Fractals* **2004**, *365*, 235–240. [CrossRef]
25. Lacan, F.; Tresser, C. Fractals as objects with nontrivial structures at all scales. *Chaos Soliton Fractals* **2015**, *75*, 218–242. [CrossRef]
26. Parvate, A.; Satin, S.; Gangal, A.D. Calculus on fractal curves in Rn. *Fractals* **2011**, *19*, 15–27. [CrossRef]
27. Chen, W. Time-space fabric underlying anomalous diffusion. *Chaos Soliton Fractals* **2006**, *28*, 923–929. [CrossRef]
28. Tarasov, V.E. General Fractional Vector Calculus. *Mathematics* **2021**, *9*, 2816. [CrossRef]
29. Li, J.; Ostoja-Starzewski, M. Micropolar mechanics of product fractal media. *Proc. R. Soc. A* **2022**, *478*, 20210770. [CrossRef]
30. Balankin, A.; Baltasar, M. Vector differential operators in a fractional dimensional space, on fractals, and in fractal continua. *Chaos Solitons Fractals* **2023**, *168*, 113203. [CrossRef]
31. Malcherek, A. History of the Torricelli principle and a new outflow theory. *J. Hydraul. Eng.* **2016**, *142*, 02516004. [CrossRef]
32. Balankin, A.S.; Elizarraraz, B.E. Hydrodynamics of fractal continuum flow. *Phys. Rev. E* **2012**, *85*, 025302(R). [CrossRef]
33. Balankin, A.S.; Elizarraraz, B.E. Map of fluid flow in fractal porous medium into fractal continuum flow. *Phys. Rev. E* **2012**, *85*, 056314. [CrossRef]
34. Balankin, A.; Patino, J.; Patino, M. Inherent features of fractal sets and key attributes of fractal models. *Fractals* **2022**, *30*, 2250082. [CrossRef]
35. Balankin, A.S. Fractional space approach to studies of physical phenomena on fractals and in confined low-dimensional systems. *Chaos Solitons Fractals* **2020**, *132*, 109572. [CrossRef]
36. Havlin, S. *Diffusion and Reactions in Fractals and Disordered Systems*; Cambridge University Press: Cambridge, UK, 2000.
37. Clanet, C. Clepsydrae, from Galilei to Torricelli. *Phys. Fluids* **2000**, *12*, 2743–2751. [CrossRef]
38. Zheng, B.; Qi, S.; Guo, S.; Liang, N.; Luo, G.; Zhang, X.; Lu, W.; Jin, C.; Li, Y.; Yu, X.; et al. Experimental Study of Direct Shear Properties of Anisotropic Reservoir Shale. *Energies* **2024**, *17*, 1997. [CrossRef]
39. Zou, S.; Xu, P.; Xie, C.; Deng, X.; Tang, H. Characterization of Two-Phase Flow from Pore-Scale Imaging Using Fractal Geometry under Water-Wet and Mixed-Wet Conditions. *Energies* **2022**, *15*, 2036. [CrossRef]
40. Maramathas, A.; Boudouvis, A. A "fractal" modification of Torricelli's formula. *Hydrogeol. J.* **2009**, *18*, 311–316. [CrossRef]
41. Balankin, A.S.; Matías-Gutierres, S.; Samayoa, D.; Patiño Ortiz, J.; Espinoza-Elizarraraz, B.; Martínez-González, C. Slow kinetics of water escape from randomly folded foils. *Phys. Rev. E* **2011**, *83*, 036310. [CrossRef] [PubMed]
42. Balankin, A.; Morales-Ruiz, L.; Matías-Gutierres, S.; Susarrey-Huerta, O.; Samayoa, D.; Patiño Ortiz, J. Comparative study of gravity-driven discharge from reservoirs with translationally invariant and fractal pore networks. *J. Hydrol.* **2018**, *565*, 467–473. [CrossRef]
43. Balankin, A.; Valdivia, J.; Marquez, J.; Susarrey, O.; Solorio-Avila, M. Anomalous diffusion of fluid momentum and Darcy-like law for laminar flow in media with fractal porosity. *Phys. Lett. A* **2016**, *380*, 2767–2773. [CrossRef]
44. Alcántara-López, F.; Camacho-Velázquez, R.; Brambila-Paz, F.; Chávez, C. Spatial fractional Darcy's law on the diffusion equation with a fractional time derivative in single-porosity naturally fractured reservoirs. *Energies* **2022**, *15*, 4837. [CrossRef]
45. Dorhjie, D.; Yusupov, R.; Krutko, V. Deviation from Darcy Law in Porous Media Due to Reverse Osmosis: Pore-Scale Approach. *Energies* **2022**, *15*, 6656. [CrossRef]
46. Samayoa, D.; Alcántara, A.; Mollinedo, H.; Barrera-Lao, F.; Torres-SanMiguel, C. Fractal Continuum Mapping Applied to Timoshenko Beams. *Mathematics* **2023**, *11*, 3492. [CrossRef]
47. Korvin, G. Menger Sponge Models. In *Statistical Rock Physics*; Springer Nature Switzerland: Cham, Switzerland, 2024; pp. 179–206. [CrossRef]
48. Cristea, L.L.; Steinsky, B. Connected generalised Sierpinski carpets. *Topol. Its Appl.* **2010**, *157*, 1157–1162. [CrossRef]
49. Balankin, A.S.; Mena, B.; Martínez, M. Hausdorff dimension and geodesic metric of critical percolation cluster in two dimensions. *Phys. Lett. A* **2017**, *381*, 2665–2672. [CrossRef]
50. Balankin, A.S. Effective degrees of freedom of a random walk on a fractal. *Phys. Rev. E* **2015**, *92*, 062146. [CrossRef]

51. Balankin, A.; Ramirez-Joachim, J.; Gonzalez-Lopez, G.; Gutierrez-Hernandez, S. Formation factors for a class of deterministic models of pre-fractal pore-fracture networks. *Chaos Soliton Fractals* **2022**, *162*, 112452. [CrossRef]
52. Patino-Ortiz, J.; Patino-Ortiz, M.; Martínez-Cruz, M.A.; Balankin, A. A Brief Survey of Paradigmatic Fractals from a Topological Perspective. *Fractal Fract.* **2023**, *7*, 597. [CrossRef]
53. Wang, F.; Jiao, L.; Liu, Z.; Tan, X.; Wang, C.; Gao, J. Fractal analysis of pore structure in low permeability sandstones using mercury intrusion porosimetry. *J. Porous Media* **2018**, *21*, 1097–1119. [CrossRef]
54. Zeng, Q.; Chen, S.; Yang, P.; Peng, Y.; Wang, J.; Zhou, C.; Wang, Z.; Yan, D. Reassessment of mercury intrusion porosimetry for characterizing the pore structure of cement-based porous materials by monitoring the mercury entrapments with X-ray computed tomography. *Cem. Concr. Compos.* **2020**, *113*, 103726. [CrossRef]
55. Park, Y.; Kim, S.; Ahn, S.e.a. Magnetic resonance imaging–based 3-dimensional fractal dimension and lacunarity analyses may predict the meningioma grade. *Eur. Radiol.* **2020**, *30*, 465–4622. [CrossRef]
56. Boming, Y.; Li, J. Some fractal character of porous media. *Fractals* **2001**, *9*, 365–372. [CrossRef]
57. Boming, Y. Fractal Character for Tortuous Streamtubes in Porous Media. *Chin. Phys. Lett.* **2005**, *22*, 158. [CrossRef]

Disclaimer/Publisher's Note: The statements, opinions and data contained in all publications are solely those of the individual author(s) and contributor(s) and not of MDPI and/or the editor(s). MDPI and/or the editor(s) disclaim responsibility for any injury to people or property resulting from any ideas, methods, instructions or products referred to in the content.